Article:
Flokstra, MG, Stewart, R, Satchell, N orcid.org/0000-0003-1597-2489 et al. (6 more authors) (2021) Meissner screening as a probe for inverse superconductor-ferromagnet proximity effects. Physical Review B, 104 (6). L060506. ISSN 2469-9950

https://doi.org/10.1103/PhysRevB.104.L060506

Meissner screening as a probe for inverse superconductor-ferromagnet proximity effects

M. G. Flokstra[1*], R. Stewart[1,4,5], N. Satchell[2], G. Burnell[2], H. Luetkens[3], T. Prokscha[3], A. Suter[3], E. Morenzoni[3] and S. L. Lee[1]

[1]*School of Physics and Astronomy, SUPA, University of St.Andrews, St.Andrews KY16 9SS, United Kingdom.* [2]*School of Physics and Astronomy, University of Leeds, Leeds LS2 9JT, United Kingdom.* [3]*Labor für Myonspinspektroskopie, Paul Scherrer Institut, CH-5232 Villigen PSI, Switzerland.* [4]*Laboratory for Mesoscopic Systems, Department of Materials, ETH Zurich, CH-8093 Zurich, Switzerland.* [5]*Laboratory for Multiscale Materials Experiments, Paul Scherrer Institute, CH-5232 Villigen PSI, Switzerland.*

(Dated: August 9, 2021)

We present experimental results on the observed flux screening in proximity coupled superconductor - ferromagnet thin film structures using Nb and Co as superconductor and ferromagnet respectively. Using the low-energy muon-spin rotation technique to locally probe the magnetic flux density we find that the addition of the ferromagnet increases the total flux screening inside the superconductor. Two contributions can be distinguished. One is consistent with the predicted spin-polarization (or magnetic proximity) effect, while the other is in line with the newly emerged electromagnetic proximity models. Furthermore, we show that the addition of a few nanometers of a normal metallic layer between the Nb and the Co fully destroys the contribution due to electromagnetic proximity. This is unanticipated by the current theory models in which the magnetization in the F layer is assumed to be the only driving force for the EM effect and suggests the role of additional factors. Further experiments to explore the influence of the direction of the F magnetization also reveal deviations from theory. These new findings are an important step forward in improving the theoretical description and understanding of proximity coupled systems.

The exotic electron pairs that can emerge at interfaces between superconducting (S) and ferromagnetic (F) regions[1, 2] allow the merging of superconductivity and spin-sensitive transport resulting in the developing field of superconducting spintronics[3–5]. In such S/F proximity systems, the essential, unique element is the presence of spin triplet pair correlations, not present in proximity systems using ordinary metals. Their odd-frequency character makes them behave in counter-intuitive ways, resulting in, for example, a paramagnetic Meissner response[6–9], while the equal-spin fractions of the triplet pairs carry a net spin and can thus be used for carrying information in superconducting spintronic devices. Furthermore these equal-spin pairs do not experience the ferromagnetic exchange field as being hostile and as a consequence can survive within such a material over much longer distances than spin-singlet correlations[10–17]. However, since these odd-frequency pairs are not eigenstates of the condensate, they are converted back into singlets inside the superconductor and therefore don't survive long inside the S layer. Their effects are thus expected to only be observable close to the (buried) S/F interface where they are generated. There are very few techniques capable of observing such effects, most notably low-energy muon-spin spectroscopy (e.g [18]), but there are also reports using polarized neutron spectroscopy[19], nuclear magnetic resonance[20] and Kerr rotation[21]. If the S layer is thin enough (a few coherence lengths, ξ_S, at most) such that triplet pairs reach the opposite side, then surface probe techniques like scanning tunneling microscopy could be used but it is not entirely clear if or how the spectra may be modified[22].

To study these proximity systems experimentally, their effects are typically measured (using standard transport techniques) around critical points like the transition temperature T_c or critical current I_c. These techniques and measurements have been very successful in understanding and developing S/F theory and in particular the propagation of superconducting pairs outside of the superconductor. However, the effect on the superconducting condensate inside the superconductor (inverse proximity) is much less studied.

It is predicted that a spin polarization can appear inside the superconductor[23] (also called a magnetic proximity effect), however, observing this (subtle) effect experimentally has proven difficult since it only exists near the interface over a distance of a few ξ_S. While some reported experiments support this prediction [20, 21], they appear to be contradicted by other detailed measurements that probe the interface region [18, 24]. These discrepancies may be explained by the newly emerging electromagnetic (EM) proximity theory models [25–27], which show a contribution to the (inverse) S/F proximity effect that has been largely overlooked for decades. In essence, it is the screening response of the superconductor to a vector potential at (or near) the S/F interface. This effect propagates over

*Corresponding author. Email: mgf@st-andrews.ac.uk

distances of the order of the magnetic penetration depth (λ), which for thin films of Nb can be much longer than ξ_S. It provides understanding for experimental results which could not be explained by previous S/F models. It also predicts a dominant contribution to the inverse S/F proximity effect in the absence of any applied field and could be used for switchable S/F devices by means of temperature alone. More generally, it shows how the presence of a local gradient in the vector potential at the S/F interface propagates into the superconductor by means of spontaneous superconducting currents. This in turn raises the interesting questions of how to manipulate this vector potential, or perhaps even how to generate it by other means.

In this paper we use the flux expulsion inside the superconductor as a probe of the inverse proximity effects in S/F systems and find an oscillatory behavior as a function of the F layer thickness. While this is predicted by the EM theory, we also present other data that suggest this description to be incomplete due to deviations from this new model. This suggests additional influences, such as spin-orbit interactions, which could also act as sources of effective vector potential. We also show that while the addition of the very thin metallic layers appears to switch off the EM effect, there remains a short-range effect consistent with the predicted spin polarization.

All our samples were prepared by dc magnetron sputtering in a system with a base pressure of 10^{-8} mbar at an ambient temperature. We use Nb as the superconductor, which depending on the Nb target quality results in a magnetic penetration depth of 160 nm (higher purity target) or 270 nm (lower purity target), see [28]. For both Nb targets, the superconducting transition temperature (T_c) of sputtered Nb films is about 8.7 K and the superconducting (Ginzburg–Landau) coherence length around 10 nm (lower purity) and 11.1 nm (higher purity).

To study the S/F proximity effect inside the superconductor, we use the low-energy muon-spin rotation (LE-μSR) technique to probe locally the magnetic flux. Compared to the more common bulk μSR, where muons penetrate the sample over the micrometer range, for LE-μSR the muon energy is moderated down to the keV range, which allows the control of the implantation depth of muons into the sample in the 10 to 100 nm range [29], where the precise stopping depth can be calculated using a well-proven Monte Carlo simulation [30, 31]. This technique has proven very successful in studying novel effects in S/F proximity systems. During a LE-μSR experiment, 100 % spin-polarized muons, which have a lifetime of 2.197 μs, are implanted into the sample one at a time. Once implanted, the muon spin starts precessing around the local magnetic flux density with a frequency directly related to the local magnetic flux density, until it decays emitting a positron. The essence of the muon technique is that this precession can be monitored by measuring the decay positron that is emitted (preferentially) along the muon spin direction at the moment of decay. All our LE-μSR measurements were performed on the μE4 beam-line at the Paul Scherrer Institut[32] using the transverse field geometry (field applied orthogonal to the muon spin direction) with the applied field direction in the plane of the sample. The measurement field was set to 300 Oe and the lateral sizes of our samples were about 2×2 cm^2 such that they capture the full muon beam, which is roughly 2 cm in diameter.

From the measurement data taken at a particular energy E, and thus a particular stopping depth $\langle x\rangle$, one can determine the average flux density $\langle B\rangle(\langle x\rangle)$. Alternatively, one can impose a model function for the flux density profile $B(x, a_i)$ onto the data, with a_i the (fit)parameters describing the profile in order to find best fit values for a_i to match the measurement data (see e.g. [28]). For example, in the case of an isolated Nb film (in the dirty limit) the flux profile is the well-known Meissner profile with the magnetic penetration depth λ the only unknown fit parameter, which can thus be obtained in this way. For the S/F bilayers, the EM-theory model predicts an exponentially decaying contribution to this Meissner profile with a maximum amplitude (A_{EM}) at the Nb/Co interface and a characteristic decay length of λ, thus adding only the amplitude as an extra fitparameter.

The EM effect has the ability to both add and subtract to the contributions to the screening due to the applied field. This depends on both the variation of the thickness of the F layer and on the sign of the magnetization. For the thickness dependence in the diffusive limit, an oscillatory behavior of the effect is predicted with a characteristic length of the order of ξ_F, the coherence length inside the F layer [25]. In what follows, we will first show the measured thickness dependence of the effect before presenting results on the magnetization direction dependence.

To examine the (inverse) S/F proximity effect we prepared a series of Nb/Co bilayer samples with varying Co thickness while keeping the Nb layer thickness at 90 nm. The Co thickness was varied from 1 nm up to 3 nm, coinciding with the expected ξ_F of about 1 nm for the Co layer. Figure 1 shows the LE-μSR results obtained on the bilayer with a Co thickness of 1.5 nm. The top panel of the figure shows the muon stopping profiles at several implantation energies for this sample. Since even at the highest energies used only a small fraction of muons get past the Nb layer, the stopping profiles for the samples with different Co thicknesses are near identical. The bottom panel shows the $\langle B(\langle x\rangle)\rangle$ obtained with open/closed symbols presenting the data taken at $T = 10$ K (with Nb in the normal state) and $T = 2.5$ K respectively. Error bars for $\langle B(\langle x\rangle)\rangle$ are plotted for all measurements but are typically too small (0.1–0.3 G) to be seen. At 10 K the LE-μSR measurements simply recover the applied measurement field while at 2.5 K a clear flux screening appears inside the Nb. These results are consistent with previous measurements reported in [33, 34] where for sample preparation the same Nb targets were used

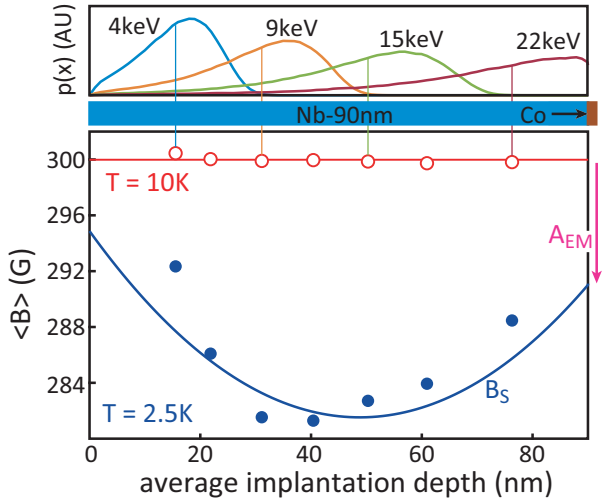

FIG. 1: Results for the Nb(90nm)/Co(1.5nm) bilayer. Top panel: Muon stopping profiles for several implantation energies with their respective average implantation depth marked on the x axis. For a muon energy of 22 keV a (small) tail extends into the Co and Si substrate (not shown). Bottom panel: LE-μSR results showing the average flux as a function of muon penetration depth obtained using a measurement field of approximately 300 Oe. Open/closed symbols represent measurements taken at $T = 10$ K (with Nb in the normal state) and $T = 2.5$ K respectively. Curve B_S is the best obtained fit solution for $B(x)$ when using the EM proximity model with A_{EM} the strength of the effect at the interface.

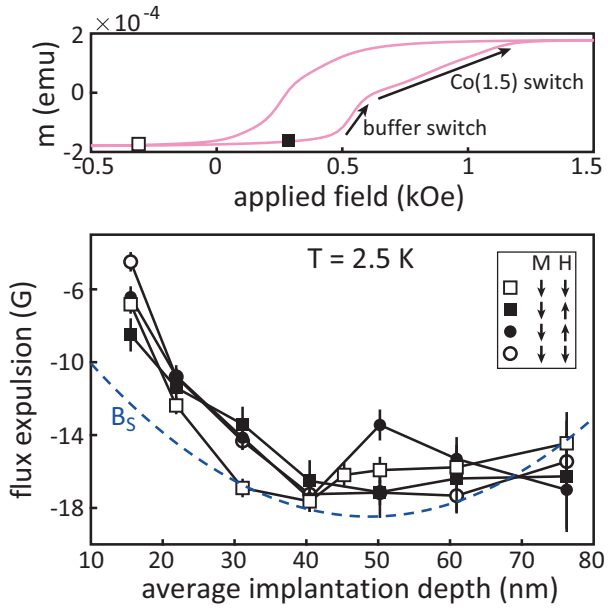

FIG. 3: Top panel: magnetization behavior of our exchange biased sample taken at $T = 10$ K, indicating the magnetic states at which LE-μSR measurements were performed. Bottom panel: LE-μSR results showing the flux expulsion as function of muon penetration depth, measured at $T = 2.5$ K, when applied field is parallel(open symbols) or anti-parallel(close symbols) to the magnetization direction of the pinned Co layer. For direct comparison the result for B_s from Fig.1 is added as a dashed line

with identical growth parameters. Analyzing the 2.5K data within the EM-theory model (see [33] for details on the precise fit functions used) shows an amplitude of about 8 G at the Nb/Co interface. Applying the above analysis to all the bilayer samples of this set yields the results shown in Fig. 2. A clear oscillatory behavior as a function of Co layer thickness is obtained, with an oscillation period (and damping) of the order of the coherence length inside the Co (~ 1 nm).

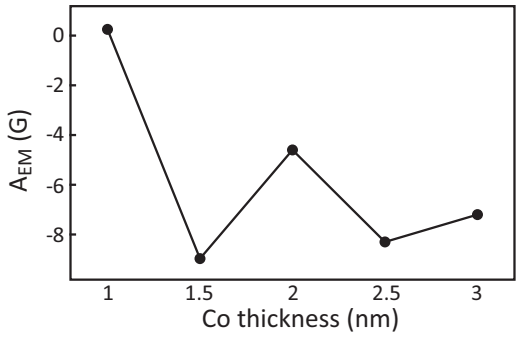

FIG. 2: LE-μSR results on the Nb(90nm)/Co(x) sample series, showing the amplitude A_{EM} of the EM model as function of Co layer thickness. The error in the obtained fitparameters are smaller than the used marker size and thus not visible.

The predicted oscillation of the EM model [25] is thus clearly visible, however, the EM model also predicts the sign of the amplitude A_{EM} to be sensitive to the direction of magnetization in the Co layer [25] (i.e. switching the magnetization from $+\mathbf{M}$ to $-\mathbf{M}$ should give a sign change of A_{EM}). To investigate this we add to the Nb/Co layer a thin IrMn layer, which is an anti-ferromagnet and can be used to pin the magnetization in the Co layer along a determined axis. To determine the pinning direction and enhance its properties, the IrMn itself is grown in a field, on top of a thin Co (buffer) layer. The full sample layout is Nb(90)/Co(1.5)/IrMn(4)/Co(3)/Ta(4.5)/Si-substrate with numbers indicating the layer thickness in nm, where Ta(4.5) acts as a seed layer to improve growth quality. The magnetization behavior of this sample, measured at $T = 10$ K, is shown in the top panel of Fig.3. Starting at saturation in negative field bias, first the Co buffer layer switches at around 500 Oe after which it requires about 1.2 kOe before the Co(1.5) layer is fully switched. The open/closed squares mark the -300/+300 Oe field values which respectively have both the field and the net magnetization either parallel or anti-parallel to the magnetization in the Co(1.5) layer. The bottom panel of the figure shows the results of the LE-μSR measurement taken at these two fields, as well as the result when coming from positive saturation instead (circle symbols),

presenting the $\langle B\left(\langle x\rangle\right)\rangle$ obtained. Similar to the sister sample without the IrMn layer (dashed line in the figure for a direct comparison), at higher muon energies a significant flux screening is still observed showing a significant contribution to the flux screening originating from the Nb/Co interface region. However, we do not observe the predicted sign change for A_{EM}. In fact, all measurements are identical within a few standard deviations. This then raises the question of whether there is another, more dominant source (compared to $\mathbf{M}$) responsible for the required gradient in the vector potential, which is not sensitive to the direction of $\mathbf{M}$.

To further investigate this possibility we modify our systems by inserting a normal metallic spacer layer, of a few nanometer thickness, between the Nb and Co. In one case we use Cu, which we previously have used to show Meissner screening propagating into the Cu over long distances[28] (see the Supplemental Materials[41] for propagation lengths of at least 90 nm). In the other case we use Pt, which has a high spin-orbit coupling strength and short spin diffusion length, both opposite to the properties of Cu. We also replace the 90 nm Nb by a Cu/Nb bilayer to highlight the compatibility of Cu with induced Meissner screening in our structures[28, 33, 34]. The full sample layouts are Cu(40)/Nb(50)/X(2)/Co(2.4)/Nb(3)/Si-substrate, with numbers indicating the layer thickness in nm, X either Cu or Pt, and the Nb(3) a non-superconducting seed layer to improve growth quality. The results of measurements on these samples are presented in Fig.4. The top panel of the figure shows several examples of muon stopping profiles for a Cu(40)/Nb(50) bilayer. At the highest energies used, only a small fraction of muons get past the Nb layer, which makes the stopping profiles for all samples presented in the figures nearly identical.

In the center panel the LE-μSR results for the Cu-spacer sample are shown together with its control samples; a Cu/Nb bilayer (NS) and Cu/Nb/Co trilayer (NSF) for direct comparison. Similarly, the results for the Pt-spacer sample are shown in the bottom panel. In both cases, the addition of the thin spacer layer has a very similar effect with two notable features. Firstly, it almost completely kills off the additional (EM proximity) flux expulsion across the sample due to the presence of the F layer (the NSF control sample shows a clear screening enhancement when compared with the NS control sample). Secondly, near the S/F interface there remains an additional more localized flux lowering compared to the bilayer case. The propagation of the latter appears to be of the order of the superconducting coherence length, which makes it, in appearance, consistent with the magnetic proximity effect predicted by Bergeret and co-workers[23]. We note that the relatively large difference in Meissner screening between the Cu-spacer and Pt-spacer system is due to the underlying 160 nm vs 270 nm penetration depth for the two sets of samples which were grown using different

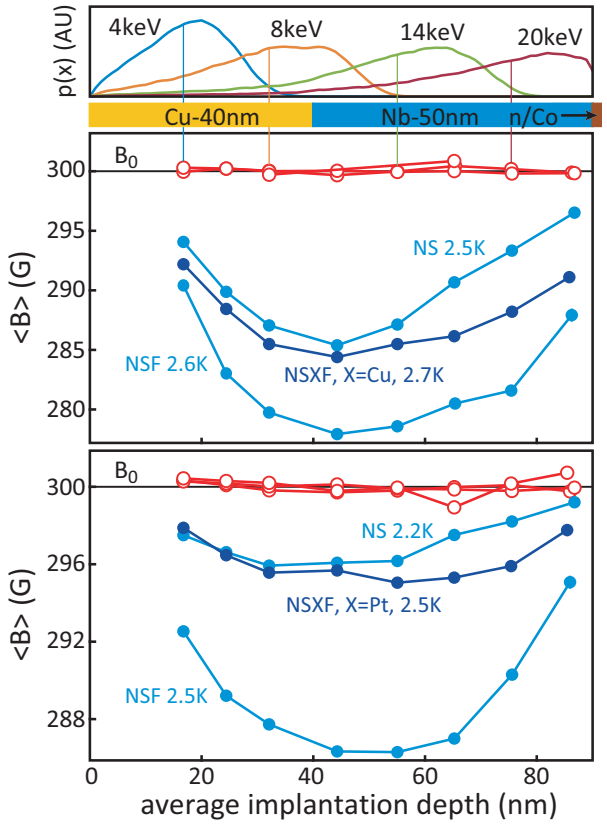

FIG. 4: Top panel: Muon stopping profiles for a Cu(40nm)/Nb(50nm) bilayer for several implantation energies with their respective average implantation depth marked on the x axis. Only for $E = 20$ keV and above a (small) tail extend into the Si substrate (not shown). Center/Bottom panel: LE-μSR results showing the average flux as function of muon penetration depth obtained for the Cu-spacer/Pt-spacer sample as well as their respective control samples: Cu/Nb bilayers (NS) and Cu/Nb/Co trilayers (NSF). Open/closed symbols present measurements taken at $T = 10$ K (with Nb in the normal state) and $T \sim 2.5$ K. Results on some of the control samples have been published before[28, 33] and serve only as a direct comparison for the Cu and Pt spacer samples.

Nb target purities. Furthermore, the temperatures used to measure in the superconducting state deviate slightly from one another but this has negligible impact since the $\langle B\rangle\left(T\right)$ has a near linear behavior and at the measured temperature of about 2.5 K, a 0.2 K deviation only accounts for about 4% of the observed flux expulsion (see e.g. [28]).

We thus observe two additional contributions to the flux screening as a result of mixing the superconducting order with the ferromagnetic order, both of which enhance the screening and originate from near the interface region between the two orders. However, the distances over which these additions propagate are very different and seem to be of the order of ξ_S for the first and λ

for the second. The first contribution is fully consistent with the predicted spin-polarization (magnetic proximity effect) while the latter we attribute to the newly emerged EM-theory, albeit with the following caveat.

The experimental evidence points towards the precise interface conditions in our Nb/Co systems being the driving mechanism of the observed EM proximity, rather than the magnetization alone. In contrast to the effect of these metallic spacer layers, in experiments using thin insulating AlO_x layers to separate the Nb from the Co we found this unusual flux screening to be unaffected, up to a thickness of about 5 nm of AlO_x[34]. One possible candidate for a contributing mechanism to explain these results is the presence of spin-orbit interactions, possibly due to the precise details of the interface. Spin orbit interactions are, from a theoretical point of view, capable of manipulating and even generating odd-frequency triplet correlations[35–37], while experimentally the existence of triplet spin currents in such systems have been implied by[38] (and e.g. [39, 40]).

Our results also show that a Cu/Nb bilayer can be more efficient at screening flux than a single Nb layer of the same total thickness, as we have shown numerically in[28]. In Fig.1 the Nb(90)/Co gives a maximum expulsion of about 18 G while the Cu(40)/Nb(50)/Co of Fig.4 (mid panel), which was grown using the same Nb target purity and measured under near identical system parameters, shows a maximum flux expulsion of about 22 G (see the Supplemental Materials[41] for a direct comparison).

In conclusion, we have investigated (inverse) superconducting proximity effects in S/F thin film structures by using LE-μSR to measure flux expulsion inside the superconducting layer. We find an oscillatory behavior of the flux expulsion as function of the F layer thickness, as predicted by the model for the EM proximity effect, but do not observe the predicted dependence on the direction of magnetization. By inserting a normal metallic spacer layer, with a thickness of only a few nanometers, between the S and F layers we observe an almost complete collapse of the EM proximity effect. This demonstrates the importance of the specifics of the materials forming the S/F contact (Nb/Co in our experiment) and hints towards a contact-specific mechanism (e.g. spin-orbit interactions) that creates the gradient in the local vector potential required for the EM proximity effect. A material specific dependence also enables a wide range of potential material choices to tune the proximity effects and allow for different architectures. Our results provide new evidence to further develop the emerging EM proximity theories.

We acknowledge the support of the EPSRC through Grants No. EP/I031014/1, No. EP/J01060X, No. EP/J010634/1, No. EP/L015110/1, No. EP/R031924/1 and No. EP/R023522/1. This project has received funding from the European Union's Horizon 2020 research and innovation programme under the Marie Skłodowska-Curie grant agreement No. 743791 (SUPERSPIN). RS acknowledges funding under ETH Zurich Postdoctoral Fellowship 20-1 FEL-36. All muon experiments were undertaken courtesy of the Paul Scherrer Institut. The research data supporting this publication can be accessed at https://doi.org/10.17630/61e3f4e4-9297-4291-8d57-8959a66f4003 [42].

[1] A. I. Buzdin, *Rev. Mod. Phys.* **77**, 935 (2005).
[2] F. S. Bergeret, A. F. Volkov, and K. B. Efetov, *Rev. Mod. Phys.* **77**, 1321 (2005).
[3] M. Eschrig, *Phys. Today* **64**(1), 43 (2011).
[4] M. Eschrig *Rep. Prog. Phys.* **78**, 104501 (2015).
[5] J. Linder and J. W. A. Robinson, *Nat. Phys.* **11**, 307 (2015).
[6] T. Yokoyama, Y. Tanaka, and N. Nagaosa, *Phys. Rev. Lett.* **106**, 246601 (2011).
[7] M. Alidoust, K. Halterman, and J. Linder, *Phys. Rev. B* **89**, 054508 (2014).
[8] A. Di Bernardo, Z. Salman, X. L. Wang, M. Amado, M. Egilmez, M. G. Flokstra, A. Suter, S. L. Lee, J. H. Zhao, T. Prokscha, E. Morenzoni, M. G. Blamire, J. Linder, and J. W. A. Robinson, *Phys. Rev. X* **5**, 041021 (2015).
[9] M. Rogers, A. Walton, M. G. Flokstra, F. Al Ma'Mari, R. Stewart, S. L. Lee, T. Prokscha, A. J. Caruana, C. J. Kinane, S. Langridge, H. Bradshaw, T. Moorsom, M. Ali, G. Burnell, B. J. Hickey, and O. Cespedes, *Commun. Phys.* **4**, 69 (2021).
[10] R. S. Keizer, S. T. B. Goennenwein, T. M. Klapwijk, G. Miao, G. Xiao, and A. Gupta, *Nature* **439**, 825 (2006).
[11] T. S. Khaire, M. A. Khasawneh, W. P. Pratt Jr., and N. O. Birge, *Phys. Rev. Lett.* **104**, 137002 (2010).
[12] J. W. A. Robinson, J. D. S. Witt, and M. G. Blamire, *Science* **329**, 59 (2010)
[13] J. W. A. Robinson, G. B. Halász, A. I. Buzdin, and M. G. Blamire, *Phys. Rev. Lett.* **104**, 207001 (2010).
[14] J. Wang, M. Singh, M. Tian, N. Kumar, B. Liu, C. Shi, J. K. Jain, N. Samarth, T. E. Mallouk, and M. H. W. Chan, *Nat. Phys.* **6**, 389 (2010).
[15] M. S. Anwar, F. Czeschka, M. Hesselberth, M. Porcu, and J. Aarts, *Phys. Rev. B* **82**, 100501(R) (2010).
[16] J. Y. Gu, J. Kusnadi, and C.-Y. You, *Phys. Rev. B* **81**, 214435 (2010).
[17] D. Sprungmann, K. Westerholt, H. Zabel, M. Weides, and H. Kohlstedt, *Phys. Rev. B* **82**, 060505(R) (2010).
[18] M. G. Flokstra, N. Satchell, J. Kim, G. Burnell, P. J. Curran, S. J. Bending, J. F. K. Cooper, C. J. Kinane, S. Langridge, A. Isidori, N. Pugash, M. Eschrig, H. Luetkens, A. Suter, T. Prokscha, and S. L. Lee, *Nat. Phys.* **12**, 57 (2016).
[19] Yu. N. Khaydukov, B. Nagy, J.-H. Kim, A. Rühm, Yu. V. Nikitenko, K. N. Zhernenkov, J. Stahn, L. F. Kiss, A. Csik, L. Bottyán, and V.L. Aksenov, *JETP Lett.* **98**, 116 (2013).
[20] R. I. Salikhov, I. A. Garifullin, N. N. Garif'yanov, L. R. Tagirov, K. Theis-Bröhl, K. Westerholt, and H. Zabel, *Phys. Rev. Lett.* **102**, 087003 (2009).
[21] J. Xia, V. Shelukhin, M. Karpovski, A. Kapitulnik, and A. Palevski, *Phys. Rev. Lett.* **102**, 087004 (2009).
[22] A. Di Bernardo, S. Diesch, Y. Gu, J. Linder, G. Divi-

tini, C. Ducati, E. Scheer, M. G. Blamire, and J. W. A. Robinson, *Nature Commun.* **6**, 8053 (2015).
[23] F. S. Bergeret, A. F. Volkov, and K. B. Efetov, *Phys. Rev. B* **69**, 174504 (2004).
[24] M. G. Flokstra, S. J. Ray, S. J. Lister, J. Aarts, H. Luetkens, T. Prokscha, A. Suter, E. Morenzoni, and S. L. Lee, *Phys. Rev. B* **89**, 054510 (2014).
[25] S. Mironov, A. S. Mel'nikov, and A. Buzdin, *Appl. Phys. Lett.* **113**, 022601 (2018).
[26] Zh. Devizorova, S. V. Mironov, A. S. Mel'nikov, and A. Buzdin, *Phys. Rev. B* **99**, 104519 (2019).
[27] A. F. Volkov, F. S. Bergeret, and K. B. Efetov, *Phys. Rev. B* **99**, 144506 (2019).
[28] M. G. Flokstra, R. Stewart, N. Satchell, G. Burnell, H. Luetkens, T. Prokscha, A. Suter, E. Morenzoni, S. Langridge, and S. L. Lee, *Phys. Rev. Lett.*, **120**, 247001 (2018).
[29] P. Bakule and E. Morenzoni, *Contemporary Physics* **45**, 203 (2004).
[30] W. Eckstein, *Computer Simulation of Ion-Solid Interactions* (Springer, Berlin, Heidelberg, New York, 1991).
[31] E. Morenzoni, H. Glückler, T. Prokscha, R. Khasanov, H. Luetkens, M. Birke, E. M. Forgan, Ch. Niedermayer, and M. Pleines, *Nucl. Instr. and Meth. B* **192**, 254-266 (2002).
[32] T. Prokscha, E. Morenzoni, K. Deiters, F. Foroughi, D. George, R. Kobler, A. Suter, and V. Vrankovic, *Nucl. Instr. and Meth. A* **595**, 317-331 (2008).
[33] M. G. Flokstra, R. Stewart, N. Satchell, G. Burnell, H. Luetkens, T. Prokscha, A. Suter, E. Morenzoni, S. Langridge, and S. L. Lee, *Appl. Phys. Lett.* **115**, 072602 (2019).
[34] R. Stewart, M. G. Flokstra, M. Rogers, N. Satchell, G. Burnell, D. Miller, H. Luetkens, T. Prokscha, A. Suter, E. Morenzoni, and S. L. Lee, *Phys. Rev. B* **100**, 020505(R) (2019).
[35] F. Konschelle, I. V. Tokatly, and F. S. Bergeret, *Phys. Rev. B* **92**, 125443 (2015).
[36] C. R. Reeg and D. L. Maslov, *Phys. Rev. B* **92**, 134512 (2015).
[37] I. V. Bobkova and A. M. Bobkov, *Phys. Rev. B* **95**, 184518 (2017).
[38] K-R. Jeon, C. Ciccarelli, A. J. Ferguson, H. Kurebayashi, L. F. Cohen, X. Montiel, M. Eschrig, J. W. A. Robinson, and M. G. Blamire, *Nature Materials* **17**, 499-503 (2018).
[39] N. Banerjee, J. A. Ouassou, Y. Zhu, N. A. Stelmashenko, J. Linder, and M. G. Blamire, *Phys. Rev. B* **97**, 184521 (2018).
[40] N. Satchell and N. O. Birge, *Phys. Rev. B* **97**, 214509 (2018).
[41] See Supplemental Material at [URL] for additional results obtained on samples using thicker normal metal layers, and for a direct comparison between the Cu(40nm)/Nb(50nm)/Co(2.4nm) and Nb(90nm)/Co(2.5) samples.
[42] Flokstra, M. G., Lee, S., Stewart, R., Satchell, N., Burnell, G., Luetkens, H., Prokscha, T., Suter, A., Morenzoni, E., 2021, Data underpinning: Meissner screening as a probe for inverse superconductor-ferromagnet proximity effects. Dataset. University of St Andrews Research Portal. https://doi.org/10.17630/61e3f4e4-9297-4291-8d57-8959a66f4003